Decadal Changes in Southern Hemisphere Winter Cyclogenesis

Jorgen S. Frederiksen
CSIRO Marine and Atmospheric Research

Carsten Frederiksen
Bureau of Meteorology Research Centre

CSIRO Marine and Atmospheric Research Paper No. 002

22 December 2005

ISSN: 1833-2331

National Library of Australia Cataloguing-in-Publication

Frederiksen, Jorgen Segerlund.
Decadal changes in southern hemisphere winter cyclogenesis.

ISBN 1 921061 12 X (pdf.).

1. Lows (Meteorology) - Australia. 2. Winter storms - Australia. 3. Rain and rainfall - Australia. 4. Climatic changes - Australia. I. Frederiksen, Carsten Segerlund. II. CSIRO. Marine and Atmospheric Research. III. Title. (Series : CSIRO Marine and Atmospheric Research ; 002).

551.6994

Enquiries should be addressed to:

Jorgen Frederiksen
CSIRO Marine and Atmospheric Research
PMB1 ASPENDALE VIC 3195
Australia
Jorgen.Frederiksen@csiro.au
Phone: 64 3 9239 4683
Fax: 64 3 9239 4444

Distribution list

Chief of Division

Operations Manager

Project Manager

Authors

Other CSIRO Staff

National Library

CMAR Libraries

Important Notice

Use of this Report

The use of this Report is subject to the terms on which it was prepared by CSIRO. In particular, the Report may only be used for the following purposes.

- this Report may be copied for distribution within the Client's organisation;
- the information in this Report may be used by the entity for which it was prepared ("the Client"), or by the Client's contractors and agents, for the Client's internal business operations (but not licensing to third parties);
- extracts of the Report distributed for these purposes must clearly note that the extract is part of a larger Report prepared by CSIRO for the Client.

The Report must not be used as a means of endorsement without the prior written consent of CSIRO.

The name, trade mark or logo of CSIRO must not be used without the prior written consent of CSIRO.

CONTENTS

ABSTRACT

The decadal changes in Southern Hemisphere winter cyclogenesis have been studied using a global two-level primitive equation instability model with reanalyzed observed basic states. We have focused on changes in the basic states that occurred in the early to mid 1970s and have employed average July basic states for the two twenty year periods 1949-1968 and 1975-1994. The early to mid 1970s was a time of quite dramatic reduction in the winter rainfall in the South West of Western Australia (SWWA) and our study aims to examine whether the rainfall changes are associated with changes in the instability of the large-scale Southern Hemisphere circulation and associated changes in cyclogenesis modes. Our primitive equation instability model incorporates the effects of cumulus convection and surface evaporation. The evaporation has been specified through a bulk aerodynamic formula and the convection through a generalized Kuo-type parameterization. The three-dimensional basic states for the two July periods have been employed and the growth rates, e-folding times, periods and structures of the dominant cyclogenesis modes have been examined. We find that the rainfall reduction over SWWA during the early to mid 1970s is associated with a reduction in the vertical mean meridional temperature gradient and in the peak upper tropospheric jetstream zonal winds near 30^o south throughout most of the Southern Hemisphere. As a consequence the atmosphere is more stable during the later period 1975-94 for latitudes around 30^o south but also more unstable further south over the Southern Ocean. These changes are reflected in the properties of the leading Southern Hemisphere cyclogenesis modes: the fastest growing mode for 1975-94 has a growth rate which is around 30% smaller than for 1949-68 and on average the 10 leading Southern Hemisphere cyclogenesis modes for 1975-94 have growth rates that are 32% smaller than for the corresponding modes for 1949-68.

Our results suggest that a primary cause of the rainfall reduction over SWWA in the period 1975-94 is the reduction of the intensity of cyclogenesis and the southward deflection of some storms and that these changes in the transient instabilities are in turn attributable to the changes in the large-scale Southern Hemisphere circulation.

1. INTRODUCTION

The early to mid-1970s was a time of major shift in the structure of the large-scale circulation of both the Northern and Southern Hemispheres (Nitta and Yamada 1989; Trenberth 1990; Allan and Haylock 1993). In the Southern Hemisphere there was a dramatic reduction in winter rainfall in the south-west of Western Australia (SWWA) associated with an increase in Perth mean sea-level pressure (MSLP) (Sadler et al. 1988; Allan and Haylock 1993; IOCI 2002). In fact, approximately 60% of the variance in SWWA winter rainfall is explained by fluctuations in Perth MSLP throughout the 1900s (Smith et al. 2000, and references therein). As well there are significant correlations between mainly inland WA winter rainfall and Indian Ocean sea surface temperatures (SSTs) (Nicholls 1989; Drosdowsky 1993; Smith 1994; Smith et al. 2000).

In the Northern Hemisphere the Pacific-North American teleconnection pattern became more dominant and persistent in winter after the 1970s with lower geopotential height at 500 hPa over the North Atlantic (Nitta and Yamada 1989; Trenberth 1990). These atmospheric circulation changes in the Northern Hemisphere have been related to an El-Nino type response in the Pacific Ocean with warmer SSTs in the eastern tropical Pacific compared with the western part of the ocean (Nitta and Yamada 1989; Trenberth 1990; Meehl and Washington 1996) and this response operates on an interdecadal time scale (Zhang et al. 1997). This so called Pacific Decadal Oscillation (PDO) or Interdecadal Pacific Oscillation (IPO) also modulates Australian climate, particularly on the east coast (Power et al. 1999; Arblaster et al. 2002). It has been suggested that both internal natural variability of the coupled ocean atmosphere system and enhanced greenhouse gas induced climate change may be responsible for recent interdecadal changes in tropical Pacific Ocean SSTs and associated circulation and rainfall changes (Meehl and Washington 1996; Knutson and Manabe 1998).

In contrast to the situation for eastern Australia, there is considerably less correlation between the Southern Oscillation Index (SOI) or the PDO and circulation and rainfall over SWWA (Smith et al. 2000 and references therein). Thus, attributing the causes, either natural or anthropogenic, of the winter circulation and rainfall changes since the 1970s in SWWA is problematic and there appears as yet no generally accepted explanation. Our purpose here is not to address this important but difficult question but to examine a second key issue, namely, the relationships between the observed changes in the mean basic state climate, before and after the mid-1970s, and the consequent changes in the transient dynamical disturbances that may be responsible for the reduction in SWWA rainfall. In this paper we examine this relationship by analysing the dynamical transients that result from the instability of observed July basic states taken from periods before and after the 1970s shift in the atmospheric circulation. Our aim is to explore whether the primary causes of the changed rainfall is due to changes in the strength or location of extratropical storms or whether changes in the other phenomena such as blocking or north-west cloud band disturbances also play an important role.

During the last two decades it has been shown that instability theory with observed basic states that have both horizontal and vertical variations in the flow fields can explain the generation mechanisms and dynamical properties of the major classes of synoptic- and large-scale atmospheric disturbances. The causes of localized cyclogenesis and the structures of the major storm tracks in both the Northern (Frederiksen 1982, 1983a; Frederiksen and Frederiksen 1992; Whitaker and Barcilon 1992; Lee 1995; Whitaker and Dole 1995) and Southern (Frederiksen 1985; Frederiksen and Frederiksen 1993a) Hemispheres have been explained. It has also been possible to explain the dynamical causes of many other atmospheric phenomena including blocking and teleconnection patterns (Frederiksen 1982, 1983b; Simmons et al. 1983;

Branstator 1985; Anderson 1991; Frederiksen and Frederiksen 1993a; Branstator and Held 1995; Frederiksen and Branstator 2001), intraseasonal oscillations and convectively coupled equatorial waves (Frederiksen and Frederiksen 1993b, 1997; Frederiksen 2002) and Australian north-west cloud band disturbances (Frederiksen and Frederiksen 1996). For our current studies of the transient instabilities growing on July global basic states for 1949-68 and 1975-94 we employ the two-level linearized primitive equation model that was developed and applied in the series of studies by Frederiksen and Frederiksen (1992, 1993a,b, 1997) (hereafter FF92, FF93a,b, FF97 respectively) and by Frederiksen (2002). The current version of the model includes a generalized Kuo-type heating parameterization that incorporates closures for both cumulus convection and evaporation-wind feedback, as outlined in Frederiksen (2002).

The plan of this paper is as follows. Section 2 contains a summary of the two-level primitive equation instability model used in this work and details the specification of the generalized Kuo-type parameterization including closures for cumulus convective heating and evaporation-wind feedback. Section 3 describes the averaged basic states for July 1949-68 and 1975-94 used in our study while in section 4 we compare instability criteria for cyclogenesis for the two basic states. In section 5 we examine the growth rates and periods of the 20 fastest growing modes for the two basic states and focus on comparisons of the growth rates and periods of the leading SH cyclogenesis modes. In section 6 we compare and contrast the structures and amplitudes of leading SH cyclogenesis modes for the two periods and relate their properties to the causes of the rainfall reduction over SWWA in the period 1975-94. Our conclusions are presented in section 7. The appendix summarizes the formulation of the generalized Kuo-type parameterization used in this study.

2. MODEL DETAILS

The transient instabilities analyzed in this study have been obtained using the two-level linearized primitive equation model that was developed and applied in a series of studies by Frederiksen and Frederiksen (1992, 1993a,b, 1997) and by Frederiksen (2002). The current version of the model includes a generalized Kuo-type heating parameterization that incorporates closures for both cumulus convection and evaporation-wind feedback, as outlined in Frederiksen (2002) and formulated in more detail in our appendix. The linearized primitive equations are described in terms of a mean perturbation streamfunction ψ, which is the average between the values at the upper (level 1) and lower (level 3) levels, a vertical shear perturbation streamfunction τ, which is half the difference between the upper and lower-level values, the lower-level perturbation velocity potential χ (equal to minus the upper-level velocity potential), and the mean and vertical shear perturbation potential temperatures θ and σ respectively.

We consider a heating profile for which the generalized Kuo-type heating projects completely onto the internal mode dynamics (see appendix). The heating due to cumulus convection and surface evaporation then only enters the linearized mean potential temperature equation and is given by

$$\tilde{Q}_\theta = -\bar{s}\nabla^2\chi + C_F\left(u^{(3)} f_u + v^{(3)} f_v\right) \qquad \textbf{(2.1)}$$

where the basic state moisture destabilization parameter is

$$\bar{s} = A_F mL\bar{q} / c_p = Q_F \bar{q}, \qquad \textbf{(2.2)}$$

and the evaporation structure functions are:

$$f_u = (\overline{q}_s - \overline{q})\overline{u}^{(3)} / \left[\left(\overline{u}^{(3)}\right)^2 + \left(\overline{v}^{(3)}\right)^2 \right]^{1/2}, \tag{2.3a}$$

$$f_v = (\overline{q}_s - \overline{q})\overline{v}^{(3)} / \left[\left(\overline{u}^{(3)}\right)^2 + \left(\overline{v}^{(3)}\right)^2 \right]^{1/2}. \tag{2.3b}$$

Here the parameters C_F and A_F are given by Eqs. (A.16) and (A.17) respectively and Q_F is an effective cumulus heating parameter defined in Eq.(A.15). Also, $u^{(3)}\left(\overline{u}^{(3)}\right)$ and $v^{(3)}\left(\overline{v}^{(3)}\right)$ are the lower-level zonal and meridional perturbation (basic state) velocities; $\overline{q}$ and $\overline{q}_s$ are the basic state specific humidity and saturation specific humidity at the lower-level respectively; L is the latent heat of condensation and m is the moisture availability factor (see appendix). We assume that $\overline{q}$ is essentially equivalent to the moisture mixing ratio $\overline{W}$.

The first term in Eq. (2.1) is the cumulus convection parameterization which, in this linearized form, gives heating for rising motion and cooling for sinking motion. The second term in Eq.(2.1) is the evaporation-wind feedback mechanism. It is slightly more general than that used by Neelin et al. (1987) in that it involves both the zonal and meridional winds. With these closures included, the linearized mean perturbation potential temperature equation becomes

$$\begin{aligned}\frac{\partial \theta}{\partial t} &= -J(\overline{\psi}, \theta) - J(\psi, \overline{\theta}) - J(\overline{\tau}, \sigma) - J(\tau, \overline{\sigma}) \\ &\quad + \nabla \cdot \overline{\sigma} \nabla \chi + \nabla \cdot \sigma \nabla \overline{\chi} - K' \nabla^4 \theta - \overline{s} \nabla^2 \chi + C_F \left(u^{(3)} f_u + v^{(3)} f_v \right)\end{aligned} \tag{2.4a}$$

where the overbar refers to the basic state. The equations for the other perturbation fields ψ, τ, χ and σ are given by:

$$\begin{aligned}\frac{\partial \nabla^2 \psi}{\partial t} &= -J(\overline{\psi}, \nabla^2 \psi) - J\left(\psi, \nabla^2 \overline{\psi} + 2\mu + \frac{1}{2}h\right) - J(\overline{\tau}, \nabla^2 \tau) - J\left(\tau, \nabla^2 \overline{\tau} - \frac{1}{2}h\right) \\ &\quad + J(\overline{\chi}, \nabla^2 \chi) + J(\chi, \nabla^2 \overline{\chi}) + \nabla \cdot \left((\nabla^2 \overline{\tau} - \frac{1}{2}h)\nabla \chi\right) + \nabla \cdot \left(\nabla^2 \tau \nabla \overline{\chi}\right) \\ &\quad + \nabla \cdot \left(\nabla^2 \overline{\chi} \nabla \tau\right) + \nabla \cdot \left(\nabla^2 \chi \nabla \overline{\tau}\right) - K \nabla^2 (\psi - \tau) - K' \nabla^6 \psi,\end{aligned} \tag{2.4b}$$

$$\begin{aligned}\frac{\partial \nabla^2 \tau}{\partial t} &= -J(\overline{\psi}, \nabla^2 \tau) - J\left(\psi, \nabla^2 \overline{\tau} - \frac{1}{2}h\right) - J(\overline{\tau}, \nabla^2 \psi) - J\left(\tau, \nabla^2 \overline{\psi} + 2\mu + \frac{1}{2}h\right) \\ &\quad + \nabla \cdot \left((\nabla^2 \overline{\psi} + 2\mu + \frac{1}{2}h)\nabla \chi\right) + \nabla \cdot \left(\nabla^2 \psi \nabla \overline{\chi}\right) \\ &\quad + K \nabla^2 (\psi - \tau) - K' \nabla^6 \tau,\end{aligned} \tag{2.4c}$$

$$\begin{aligned}\frac{\partial \nabla^2 \chi}{\partial t} &= -J(\overline{\chi}, \nabla^2 \psi) - J\left(\chi, \nabla^2 \overline{\psi} + 2\mu + \frac{1}{2}h\right) \\ &\quad - \nabla \cdot \left((\nabla^2 \overline{\psi} + 2\mu + \frac{1}{2}h)\nabla \tau\right) - \nabla \cdot (\nabla^2 \psi \nabla \tau) \\ &\quad - \nabla \cdot \left((\nabla^2 \overline{\tau} - \frac{1}{2}h)\nabla \psi\right) - \nabla \cdot \left(\nabla^2 \psi \nabla \overline{\tau}\right) \\ &\quad + \nabla^2 \left(\nabla \overline{\psi} \cdot \nabla \tau + \nabla \psi \cdot \nabla \overline{\tau} - J(\overline{\psi}, \chi) - J(\psi, \overline{\chi}) + \theta\right) \\ &\quad - K \nabla^2 \chi - K' \nabla^6 \chi,\end{aligned} \tag{2.4d}$$

$$\frac{\partial \sigma}{\partial t} = -J(\overline{\psi}, \sigma) - J(\psi, \overline{\sigma}) - J(\overline{\tau}, \theta) - J(\tau, \overline{\theta}) + \nabla \cdot \overline{\theta} \nabla \chi + \nabla \cdot \theta \nabla \overline{\chi} - K' \nabla^4 \sigma. \quad \textbf{(2.4e)}$$

Here the Jacobian

$$J(X,Y) = \frac{\partial X}{\partial \lambda}\frac{\partial Y}{\partial \mu} - \frac{\partial X}{\partial \mu}\frac{\partial Y}{\partial \lambda} \quad \textbf{(2.5)}$$

and λ is longitude, μ is sine of latitude ϕ and t is time. The strength of the diffusion is specified by K and K' which denote surface drag and biharmonic diffusion coefficients respectively. Also $h = 2\mu g A H/(RT_0)$ where H is the global topography as shown in Fig. 1d of FF93a, g is the gravitational acceleration, R is the gas constant for air, T_0 is the horizontally averaged surface temperature, and A is a vertical profile factor taken to be 1.

These equations have been non-dimensionalized by using *a*, the radius of the earth, as a length scale; Ω^{-1}, the inverse of the earth's angular speed of rotation, as a time scale; and $a^2\Omega^2/b_\kappa c_p$ as a temperature scale, where c_p is the specific heat at constant pressure and $b_\kappa = 0.124$ is a dimensionless constant. Corresponding dimensional quantities are indicated by the superscript d in the sequel.

Again, each of the perturbation fields and basic state fields is expanded in terms of spherical harmonics with the perturbations also having a time dependence $\exp(-i\omega t)$. Here *t* is the time and $\omega = \omega_r + i\omega_i$ is the complex angular frequency with ω_r being the frequency and ω_i the growth rate. This then results in a system of eigenvalue-eigenvector equations of the form

$$-i\omega \mathbf{x} = \mathbf{A}\mathbf{x} \quad \textbf{(2.6a)}$$

where

$$\mathbf{x} = (\ldots, \psi_{mn}, \ldots, \tau_{mn}, \ldots, \chi_{mn}, \ldots, \theta_{mn}, \ldots, \sigma_{mn}, \ldots)^T \quad \textbf{(2.6b)}$$

is the column vector of spherical harmonic spectral coefficients of the five field variables, *T* denotes transpose, and the matrix **A** is determined as described in FF92. A rhomboidal 15 truncation is used for both the perturbation and basic state fields in which the zonal wave number $m = -15, \ldots, 0, \ldots, 15$ and the total wave number $n = |m|, |m|+1, \ldots, |m|+15.$

3. BASIC STATES

We have examined the global Southern Hemisphere (SH) mean July climate fields for the periods 1949-1968 and 1975-1994, using the National Centres for Environmental Prediction/National Center for Atmospheric Research (NCEP/NCAR) reanalyses (Kalnay et al., 1996), and find that there are significant differences between the two periods. Most noticeable is a reduction of 17% in the peak strength of the SH subtropical jet stream (Figure 1).

Figure 1 shows the height (in pressure units) and latitudinal cross-section of the zonal wind, averaged over 100°E-130°E longitude. In both periods, there is a maximum in the zonal wind strength in the subtropics (near 30° S) at about the 200hPa pressure level. In the later period,

there is a reduction in the zonal wind of up to 9.4 ms^{-1} in this maximum. As well we note the increase in the zonal wind, particularly in the upper troposphere, near 45° S and in the main Northern Hemisphere jet core near 35° N. These changes are directly associated with changes in the Hadley circulation (not shown). There have also been substantial changes in the Walker circulation with increased upper level wind divergence in the eastern tropical Pacific in the latter period (not shown).

The thermal structure of the SH atmosphere has also changed with a significant warming south of 30° S, as shown in the vertically averaged temperature difference between the two periods in Fig. 2a. This has reduced the equator-to-pole temperature gradient particularly in the eastern hemisphere. As well the difference in the vertically average streamfunction between the two periods is associated with a change in the strength of the Antarctic Oscillation, also known as the High-Latitude Mode or Southern Hemisphere Annular Mode (Kidson 1988; Marshall et al. 2004), as shown in Fig. 2b.

The above mentioned changes would be expected to have a significant effect on the stability of the Southern Hemisphere circulation and hence on the nature of the Southern Hemisphere storms and other modes of weather variability. In fact, as detailed in this study, in the period 1975-94 the Southern Hemisphere atmosphere has generally become less unstable in those regions associated with the generation of mid-latitude storms.

The flow fields for the basic states used in this study are the monthly averaged July global fields for the periods 1949-1968 and 1975-1994 from the NCEP/NACR reanalyses. We use global 300 hPa and 700 hPa fields as representative of the upper- and lower-levels respectively and the fields of streamfunction, velocity potential and potential temperature are represented as rhomboidal wavenumber 15 spectral fields as described in FF93a. For each of the two basic states the Southern Hemisphere 300 and 700 hPa zonal winds are shown in Fig. 3 as are the corresponding changes in these winds between the two periods. We note in particular (Fig. 3a) the strong jet stream at 300 hPa stretching across southern Australia between 80° E and 120° W longitude and centered on 30° S in the 1949-68 data. For the 1975-94 basic state the subtropical jet at 300 hPa is generally weaker (Fig. 3b). The 300 hPa difference in Fig. 3c shows that the reduction in the zonal wind in the later period, of up to 7 ms^{-1} , extends across essentially the whole hemisphere in a band centered near 30° S. As well, there is a band to the south centered near 50° S with increases of up to 5.6 ms^{-1}. Again, these changes and corresponding changes at 700 hPa (Figs. 3d, 3e and 3f) are quite dramatic and representative of the systematic change that has occurred in the SH climate since the early to mid 1970s.

The transient perturbation modes experience the effects of the instability of the three-dimensional basic state fields and of cumulus convection, surface evaporation feedback, topography and dissipation. The global topography is shown in Fig. 1d of FF93a and the scale height for the topography is as described in section 2. We use drag and biharmonic diffusion coefficients with values

$$K^d = 8.39 \times 10^{-7}\,\mathrm{s}^{-1}, \tag{3.1}$$

$$K'^d = 2.338 \times 10^{16}\,\mathrm{m}^4\mathrm{s}^{-1} \tag{3.2}$$

as in our previous studies.

The strength of the cumulus heating (Eqs. (2.1) and (A.15)), is specified by

$$Q_F^d = 1500K \tag{3.3}$$

and the corresponding moisture destabilization parameter $\bar{s}$ is positive (Eq.(2.2)). For a slowly varying basic state static stability we can combine the moisture destabilization parameter with the dry static stability term in Eq. (2.4a) and define a moist static stability by

$$\bar{\sigma}_m = \bar{\sigma} - \bar{s} \,. \tag{3.4}$$

The SH moist static stability is shown in Figs. 4a, 4b and 4c respectively for the 1949-68 and 1975-94 basic states and their difference. We note that the differences in the moist static stability for the two periods is relatively minor and is therefore not expected to be as important a determinant of changes in transient instabilities as the zonal winds (Fig. 3) and horizontal temperature structure (Fig. 2a).

The strength of the evaporation-wind feedback (Eq.(2.1)) is specified by

$$C_F^d = 5 \times 10^{-4} \text{ K m}^{-1} \tag{3.5}$$

as in Frederiksen (2002). It should be noted that C_F^d in K m^{-1} has similar magnitudes to the non-dimensional drag coefficient for evaporation C_E (Eq. (A.6b)) and is identical when the Kuo parameter $(1-b) = 0.8$ (Eq. (A.16)). The evaporation-wind structure function f_u^d has most effect on the transient instabilities while f_v^d has less systematic effect as discussed in more detail in Frederiksen (2002). The function f_u^d in g kg^{-1} is shown in Figs. 4d, 4e and 4f respectively for the 1949-68 and 1975-94 basic states and their difference. We note that, as expected, f_u^d has a similar structure to the corresponding 700 hPa zonal wind for each of the basic states shown in Fig. 3 but is more confined to the subtropics. In the SH there is in general little difference in f_u^d between the two periods apart from the increased evaporation off the north-west coast of Australia.

4. INSTABILITY CRITERION FOR CYCLOGENESIS

Before carrying out the full instability calculation with the model described in section 2 it is perhaps of interest to examine the regions of likely cyclogenesis based on the simple criterion of Phillips (1954) generalized for a moist static stability $\bar{\sigma}_m^d$ and spherical geometry as used in FF93a. This criterion may be written as

$$\bar{u}^{(1)d} - \bar{u}^{(3)d} - \frac{b_\kappa c_p \bar{\sigma}_m^d}{a\Omega} \frac{(1-\mu^2)^{1/2}}{\mu^2} \geq 0, \tag{4.1}$$

where $\bar{u}^{(1)d}$ and $\bar{u}^{(3)d}$ are the upper and lower level total zonal velocities. The fact that the denominator contains the factor $\mu^2 = \sin^2\phi$ means that near the equator the criterion will always be negative and thus the criterion is primarily of relevance for the development of extra-tropical cyclogenesis. In Figs. 5a, 5b and 5c we show the regions where the instability criterion is positive for the 1949-68 and 1975-94 basic states and their difference respectively. We note the close structural similarity between the instability criteria and the corresponding extra-tropical 300 hPa zonal winds shown in Fig.3. Again we would expect a reduction of cyclogenesis in a band around 30° S extending longitudinally across most of the Southern Hemisphere including SWWA. In fact, whether the moist static stability $\bar{\sigma}_m^d$ is used in the definition of the Phillips criterion or the corresponding dry static stability $\bar{\sigma}^d$ is employed does not change our general conclusions. This may be seen by comparing Fig. 5 with the

corresponding dry criteria in Fig. 6. We note that while the instability is predicted to be stronger with the moist static stability in Figs. 5a and 5b compared with the dry static stability in Figs. 6a and 6b, as expected, the differences between 1975-94 and 1949-68 are very similar (Figs. 5c and 6c).

5. GROWTH RATES, PERIODS AND PATTERN CORRELATIONS

The large eigenvalue-eigenvector problem (2.6a) (with a 2480×2480 matrix) has been solved for both the 1949-68 and 1975-94 basic states including the parameterizations described in section 3. As in our previous studies a wide variety of modal disturbances that can be related to many aspects of atmospheric dynamics have been obtained. Here, however, our focus will be on SH cyclogenesis modes that are amongst the 20 fastest growing modes for each basic state since it is for these modes that the changes are the most dramatic.

Table 1 gives the mode number, period and e-folding times of the 20 leading modes for the 1949-68 basic state while Table 2 gives the corresponding results for the 1975-94 basic state. Also shown are the mode types and the largest pattern correlations between modes for the two basic states. Here the pattern correlations shown are the maximum over the phases of the modes and (the averages) taken over the five model fields ψ, τ, χ, θ and σ. The pattern correlations of the perturbation fields are calculated as described in appendix C of Frederiksen and Bell (1990). For a good fit, the pattern correlations as calculated require that both the real and imaginary parts of the two modes of interest are similar; this ensures that two travelling modes are similar throughout their evolution.

Table 1 shows that the leading mode for the 1949-68 basic state is a SH cyclogenesis mode and that many of the modes among the first 20 fastest growing also correspond to SH cyclogenesis. The most similar disturbance to mode1 for the 1949-68 basic state is mode 9 for the 1975-94 basic state and they have a pattern correlation of just over 0.9. However, mode 9 for 1975-94 has a growth rate that is 33% less than mode 1 for 1949-68. We also note from Tables 1 and 2 that there are considerable fewer SH cyclogenesis modes amongst the first 20 fastest growing modes for 1975-94 than for 1949-68. In fact, on average the 10 leading Southern Hemisphere cyclogenesis modes for 1975-94 have growth rates that are 32% smaller than for the corresponding modes for 1949-68.

We also note from Table 1 that for 1949-68 the first 20 modes correspond to Southern and Northern Hemisphere cyclogenesis modes apart from mode 6 which is an Antarctic teleconnection pattern. In contrast, for 1975-94, as shown in Table 2, the first 20 modes include a greater variety, because of the drop in growth rates of the SH cyclogenesis modes, including also SH blocking and north-west cloud band disturbances.

6. STRUCTURES OF SOUTHERN HEMISPHERE CYCLOGENESIS MODES

Next we examine the structures of the leading Southern Hemisphere cyclogenesis modes during the two periods of interest. Fig. 7 shows the upper level streamfunction, lower level streamfunction and upper level divergence of mode 1 for the 1949-68 basic state (at a particular phase or time) and as well the random phase ensemble average (RPEA) of these quantities defined as in Eq.(2.7) of Frederiksen (1982). The RPEA of a disturbance field is essentially the amplitude envelope within which the disturbance propagates with changing time or phase and determines in this case the structure of the storm track. We note from Figs. 7a, 7b and 7c that

the disturbance has a wavenumber of around 12 in the regions of large amplitude over southern Australia and consists of a series of eastward propagating troughs (cool colours) and ridges (warm colours). As the troughs and ridges move eastward they amplify to reach a maximum in preferred regions of large RPEA amplitude. In Figs. 7d, 7e and 7f the amplitude variations of the storm mode are more evident with all the fields shown having largest amplitude focused over south-western Australia and secondary maxima over the central Southern Pacific Ocean. From the appendix, we note that the precipitation (A.4) due to convection is essentially determined by the lower level vertical velocity in pressure coordinates and in our model this is proportional to the magnitude of the upper level divergence. Thus, the pattern of RPEA divergence in Fig. 7f is also the expected pattern of rainfall associated with this mode, and as we have noted above the maximum is focused over south-western Australia.

For the 1975-94 basic state mode 1 in Table 2 is a Northern Hemisphere storm track mode (not shown) with largest amplitudes in streamfunction fields over the central Northern Pacific Ocean near 170° E and 45° N. The leading SH cyclogenesis mode for this 1975-94 basic state is mode 8, which as noted in section 5 has a growth rate that is around 30% less than for mode 1 for the 1949-68 basic state. Fig. 8 shows the same fields as in Fig. 7 but for mode 8 for the 1975-94 basic state. We note from Figs. 8a, 8b and 8c that the upper and lower level disturbance streamfunctions and upper level divergence have quite different structures to mode 1 for the 1949-68 basic state. Mode 8 for the 1975-94 basic state effectively bypasses south-western Australia and has maximum impact over the central Southern Pacific Ocean. These findings are perhaps most evident in the RPEA of these fields shown in Figs. 8d, 8e and 8f that exhibit primary maxima of the storm tracks near 120° W and between 30° and 40° S. We also note that mode 8 has longer period and somewhat larger scale structure than mode 1 for the 1949-68 basic state. In fact, as seen from Table 2, mode 8 for the 1975-94 basic state is most similar to mode 20 for the 1949-68 basic state, with a pattern correlation of 0.5659; for these modes that largely miss Australia there is negligible differences in their growth rates.

There are, however, other subdominant weather modes for the 1975-94 basic state, with a similar structure and period to mode 1 for the earlier stage. Mode 9 for the later basic state is the fastest growing of this group of modes and also has the largest pattern correlation (0.9148) with mode 1 for the earlier stage as shown in Table 1. Fig. 9 again shows the same disturbance fields as in Fig. 7 but for mode 9 for the 1975-94 basic state. It is clear that the modal structures shown in Fig. 9 are quite similar to those in Fig. 7, as quantified by the pattern correlation that is larger than 0.9. However, as noted in section 5, the growth rate for mode 9 for the 1975-94 basic state is around 30% less than for mode 1 for the earlier stage and this is consistent with the observed reduction in rainfall over southern Australia, and in particular, SWWA. We also note that in the later time period the impact of the cyclogenesis has shifted slightly downstream or eastward (25° in longitude from (35° S, 125° E) to (35° S, 150° E)) as seen particularly by comparing the RPEA upper level streamfunction fields in Figs. 7d and 9d.

The general properties of the storm modes outlined above are also characteristic of many of the other SH cyclogenesis modes listed in Tables 1 and 2. Importantly, as detailed in section 5, the 10 leading Southern Hemisphere cyclogenesis modes for 1975-94 have growth rates that are on average 32% smaller than for the corresponding modes for 1949-68 and this reduction is particularly notable for storm modes crossing south-western Australia.

These results again suggest that a primary cause of the rainfall reduction over SWWA in the period 1975-94 is the reduction in the intensity of cyclogenesis due to a reduction in the baroclinic instability of the large-scale Southern Hemisphere circulation. There are also some changes in other mode types between the two periods but they are less important and will not be detailed here.

7. DISCUSSION AND CONCLUSIONS

The aim of this paper has been to examine the decadal changes in the instability properties of the Southern Hemisphere winter large-scale flow, before and after the early to mid 1970s, and the associated changes in the structures and growth rates of leading SH cyclogenesis modes. Our study has been motivated by the dramatic reduction in average winter rainfall in the South West of Western Australia that occurred after the mid 1970s. We have noted that in the period 1975-94 there has been a reduction of about 9 ms^{-1} in the strength of the July peak subtropical zonal wind, near 30° S and at the 200 hPa pressure level, compared with the period 1949-68. This has been related to a significant warming of the SH troposphere south of 30° S, resulting in a reduction of the equator-to-pole temperature gradient in the latter period. There have also been significant changes in both the Hadley and Walker circulations. Changes in the dry and moist static stability and in surface evaporation in contrast appear to be less significant.

We have examined the associated changes between the two periods in the Phillips (1954) criteria for baroclinic instability, for both dry and moist static stability and generalized for spherical geometry as used in FF93. In the SH mid latitudes these instability criteria for storm generation reflect closely the strength of the upper tropospheric zonal winds. Both dry and moist differences in the criteria show a reduction in the likely cyclogenesis after the mid 1970s in a band around 30° S and stretching longitudinally across most of the Southern Hemisphere including SWWA. As well there are bands of increased likelihood of cyclogenesis at southern latitudes of the SH, particularly between Australia and Antarctica, and in the Northern Hemisphere Asian and Pacific storm tracks.

A particular focus of our work has been to perform detailed examinations of the decadal changes in SH winter cyclogenesis using the global two-level primitive equation instability model with the 1949-68 and 1975-94 NCEP/NCAR reanalyzed observed July basic states. Our study has also included the effects of topography, cumulus convection, evaporation and dissipation. The cumulus convection has been specified through a generalized Kuo-type parameterization and the evaporation through a bulk aerodynamic formula. We have examined the growth rates, e-folding times, periods and structures of dominant cyclogenesis modes based on the primitive equation instability calculations.

For the 1949-68 basic state the fastest growing mode is a SH cyclogenesis mode consisting of a series of eastward propagation troughs and ridges and with zonal wavenumber of about 12 in the regions of large amplitude over southern Australia. Peak amplitudes of streamfunctions and divergence, and therefore rainfall, are located over and near SWWA. In contrast for the 1975-94 basic state the fastest growing mode is a NH cyclogenesis mode with maximum amplitude in the Northern Pacific storm track and the first mode corresponding to SH cyclogenesis is the eighth fastest growing disturbance, mode 8. This mode has a growth rate that is about 30% less than for mode 1 for the 1949-68 basic state, is of larger scale, and moreover effectively bypasses south-western Australia and instead has maximum impact over the central Southern Pacific Ocean. The second mode corresponding to SH cyclogenesis in the latter period is mode 9 and it is much more similar to mode 1 for the 1949-68 basic state, with pattern correlation around 0.9. Mode 9 for the latter stage however has a growth rate that is 33% less than that for mode 1 for the earlier time period and the impact of the cyclogenesis has shifted slightly eastward (25° in longitude from (35° S, 125° E) to (35° S, 150° E)).

We have also found that the general properties of the few leading SH storm modes discussed above are characteristic of many of the other SH cyclogenesis modes. In particular, the 10 leading SH cyclogenesis modes for 1975-94 have on average growth rates that are 32% smaller

than for the corresponding modes for 1949-68. Further, this reduction in the latter period is especially notable for cyclogenesis modes crossing south-western Australia.

There may be other contributing causes to the observed rainfall reduction over SWWA since the mid 1970s such as changes to the land surface and associated fluxes due to land clearing (IOCI 2002). However, the reduction in the intensity of cyclogenesis and the related changes in the instability properties of the large scale Southern Hemisphere circulation are so dramatic that we conclude that they are the primary cause of the rainfall reduction.

While the observed changes in the SH climate, including the reduction in the equator-to-pole tropospheric temperature gradient and consequent zonal flow reduction in the latter period, are not inconsistent with climate change due to anthropogenic forcing from increasing greenhouse gases, this has not at this stage been established. We hope in future studies to examine this and other possible causes for the large changes in the Southern Hemisphere large scale circulation and transient instabilities that have occurred since the mid 1970s.

Acknowledgments

It is a pleasure to thank Steve Kepert for assistance with this work. This work was partly funded by the Indian Ocean Climate Initiative of the W.A. Department of Environment, Water and Catchment Protection and by the Australian Greenhouse Office and contributes to the research effort of the CSIRO Water for Healthy Country Flagship.

APPENDIX. GENERALIZED KUO CUMULUS PARAMETERIZATION

In pressure coordinates, the large-scale equations for potential temperature Θ and specific humidity q are (Molinari 1985)

$$\frac{\partial \Theta}{\partial t} + \nabla \cdot (\mathbf{v}\Theta) + \frac{\partial}{\partial p}(w\Theta) = \left(\frac{p_{1000}}{p}\right)^{\kappa} \frac{Q(p)}{c_p} \qquad \textbf{(A.1)}$$

$$\frac{\partial q}{\partial t} + \nabla \cdot (\mathbf{v}q) + \frac{\partial}{\partial p}(wq) = -C^* + g\frac{\partial F_q}{\partial p} \qquad \textbf{(A.2)}$$

with

$$Q(p) = LC^*. \qquad \textbf{(A.3)}$$

Here, $\kappa = R/c_p$, $c_p = 1004$ J K^{-1} kg^{-1} is the specific heat of air at constant pressure, $R = 287$ K^{-1} kg^{-1} is the gas constant for air, $L = 2.5\times10^6$ J kg^{-1} is the latent heat of condensation, $g = 9.8$ m s^{-2} is the gravitational acceleration, p_{1000} = 1000 hPa, p is pressure, $\mathbf{v}$ is the vector horizontal wind, $w = dp/dt$ is the vertical velocity in pressure coordinates and $Q(p)$ is the heating rate. Also, C^* is the condensation minus evaporation rate, F_q represents the boundary-layer turbulent flux of moisture and for this study we shall ignore the radiative heating rate and boundary-layer turbulent fluxes of heat.

The rate of precipitation P reaching the surface of the atmosphere is

$$P = \frac{1}{g}\int_o^{p_{1000}} dp\, C^*. \qquad \textbf{(A.4)}$$

Kuo (1974) assumed that a proportion $(1-b)$ of the total convergence of moisture, or "moisture accession", M_t, is condensed and precipitated out as rain or carried away and the fraction b increases the humidity of the air. Here

$$M_t = -\frac{1}{g}\int_o^{p_{1000}} dp \nabla \cdot (\mathbf{v}q) + E \qquad \textbf{(A.5)}$$

where the surface evaporation rate is

$$E = F_q(p_{1000}). \qquad \textbf{(A.6a)}$$

The surface evaporation is parameterized by the bulk aerodynamic form

$$E = C_E \rho(p_{1000}) |\mathbf{v}(p^*)| (q_s(p_{1000}) - q(p^*)) \qquad \textbf{(A.6b)}$$

where p^* is a level closest to the surface, C_E is a non-dimensional drag coefficient and $\rho(p_{1000}) = 1.276$ kg m^{-3} is the surface density of air.

In this paper, we shall follow modifications to the Kuo scheme proposed by Kanamitsu (1975) and Krishnamurty et al. (1976). They wrote the moisture accession in the approximate form

$$M_t = -\frac{1}{g}\int_o^{p_{1000}} dp\, w\frac{\partial q}{\partial p} + E \qquad \textbf{(A.7)}$$

obtained from the continuity equation and assuming that q is slowly varying. Further, we follow Molinari (1985) and replace Kuo's relaxation of the potential temperature towards a moist adiabat by a prescribed heating profile and introduce a similar profile of moistening into the moisture equation. Thus,

$$Q(p) = gL(1-b)M_t\eta(p) \qquad \textbf{(A.8)}$$

and

$$\frac{\partial q}{\partial t} + \nabla\cdot(\mathbf{v}q) + \frac{\partial}{\partial p}(wq) = -g(1-b)M_t\eta_q(p)\,. \qquad \textbf{(A.9)}$$

The normalized heating profile $\eta(p)$ satisfies

$$\int_o^{p_{1000}} dp\,\eta(p) = 1 \qquad \textbf{(A.10)}$$

and the moistening profile $\eta_q(p)$ is similarly normalized.

For the two-level model, $|w|$ increases linearly from $|w_0| = |w(p_0)| = 0$ to $|w_2| = |w(p_{500})|$ with increasing p and decreases linearly from $|w_2|$ to $|w_4| = |w(p_{1000})|$ with p. Also, for simplicity we assume that $q = 0$ for $p \le p_{500}$ and q increases linearly with p to $q(p_{1000})$; the condensation level is taken to be $p_{750} = 750$ hPa . The pressure spacing is $\Delta p = 250$ hPa . The moisture accession then becomes

$$M_t = \frac{-2w(p_{750})q(p_{750})}{g} + E \qquad \textbf{(A.11)}$$

and the heating entering the vertical mean (θ) and shear (σ) potential temperature equations is given by (FF93a)

$$\tilde{Q}_\theta = \frac{1}{2}\left[\tilde{Q}_\Theta(p_{250}) + \tilde{Q}_\Theta(p_{750})\right], \qquad \textbf{(A.12a)}$$

$$\tilde{Q}_\sigma = \frac{1}{2}\left[\tilde{Q}_\Theta(p_{250}) - \tilde{Q}_\Theta(p_{750})\right] \qquad \textbf{(A12b)}$$

with

$$\tilde{Q}_\theta = \left(\frac{p_{1000}}{p}\right)^\kappa \frac{Q(p)}{c_p}. \qquad \textbf{(A.13)}$$

As in FF93a, the heating profile is chosen such that the heating projects completely onto the internal mode; that is, $\tilde{Q}_\sigma$ vanishes. Also proceeding as in appendix A of FF93a we find that

$$\tilde{Q}_\theta = -\frac{Q_F}{\Delta p}q(p_{750})w(p_{750}) + C_F\left|\mathbf{v}(p^*)\right|(q_s(p_{1000}) - q(p^*)) \qquad \textbf{(A.14)}$$

where

$$Q_F = \frac{2(1-b)A_F L}{c_p} = \frac{mA_F L}{c_p}, \tag{A.15}$$

$$C_F = \frac{C_E \rho(p_{1000}) g (1-b) A_F L}{\Delta p \, c_p} \tag{A.16}$$

Also, $m = 2(1-b)$ is the moisture availability factor and

$$A_F = \left[\left(\frac{p_{750}}{p_{1000}} \right)^{\kappa} + \left(\frac{p_{500}}{p_{1000}} \right)^{\kappa} + \left(\frac{p_{250}}{p_{1000}} \right)^{\kappa} \right]^{-1}$$
$$= 0.414. \tag{A.17}$$

Now, the linearized expression for $\tilde{Q}_\theta$ given in Eq.(2.1) is obtained by approximating the velocity at p^* by one half the value at 750 hPa and q_s at 1000 hPa and q at p^* by twice their values at 750 hPa. Note also that the 750 hPa divergence is just Δp times the 750 hPa vertical velocity.

TABLE CAPTIONS

FIGURE CAPTIONS

8. REFERENCES

Allan, R.J. and M.R. Haylock, 1992: Circulation features associated with the winter rainfall decrease in southwestern Australia. *J. Climate,* **6,** 1356-1367.

Anderson, J.L., 1991: The robustness of barotropic unstable modes in a zonally varying atmosphere. *J. Atmos. Sci.,* **48**, 2393-2410.

Arblaster, J.M., G.A. Meehl and A.M. Moore, 2002: Interdecadal modulation of Australian rainfall. *Clim. Dyn.,* **18,** 519-531.

Branstator, G., 1985: Analysis of general circulation model sea-surface temperature anomaly simulations using a linear model. Part II: Eigenanalysis. *J. Atmos. Sci.,* **42**, 2241-2254.

Branstator, G. and I. Held, 1995: Westward propagating normal modes in the presence of stationary background waves. *J. Atmos. Sci.,* **44**, 247-262.

Drosdowsky, W., 1993: Potential predictability of winter rainfall over southern and eastern Australia using Indian Ocean sea-surface temperature anomalies. *Aust. Met. Mag.,* **42,** 1-6.

Frederiksen, C.S., and J.S. Frederiksen, 1992: Northern Hemisphere storm tracks and teleconnection patterns in primitive equation and quasi-geostrophic models. *J. Atmos Sci.,* **49**, 1443-1458.

Frederiksen, C.S., and J.S. Frederiksen, 1996: A theoretical model of northwest cloudband disturbances and southern hemisphere storm tracks: The role of SST anomalies. *J. Atmos. Sci.*, **53**, 1410-1432.

Frederiksen, J.S., 1982: A unified three-dimensional instability theory of the onset of blocking and cyclogenesis. *J. Atmos. Sci.*, **39**, 969-987.

Frederiksen, J.S., 1983a: Disturbances and eddy fluxes in Northern hemisphere flows: Instability of three-dimensional January and July flows. *J. Atmos. Sci.*, **40**, 836-855.

Frederiksen, J.S., 1983b: A unified three-dimensional instability theory of the onset of blocking and cyclogenesis. II: Teleconnection patterns. *J. Atmos. Sci.*, **39**, 969-987.

Frederiksen, J.S., 1985: The geographical locations of Southern Hemisphere storm tracks: Linear theory. *J. Atmos. Sci.*, **42**, 710-723.

Frederiksen, J.S., 2002: Genesis of intraseasonal oscillations and equatorial waves. *J. Atmos. Sci.*, **59**, 2761-2781.

Frederiksen, J.S., and P.J. Webster, 1988: Alternative theories of atmospheric teleconnections and low-frequency fluctuations. *Rev. Geophys.*, **26**, 459-494.

Frederiksen, J.S., and R.C. Bell, 1990: North Atlantic blocking during January 1979: Linear theory. *Q.J.R. Meteorol. Soc.*, **116**, 1289-1313.

Frederiksen, J.S., and C.S. Frederiksen, 1993a: Monsoon disturbances, intraseasonal oscillations, teleconnection patterns, blocking and storm tracks of the global atmosphere during January 1979: Linear theory. *J. Atmos. Sci.*, **50**, 1349-1372.

Frederiksen, J.S. and C.S. Frederiksen, 1993b: Southern Hemisphere storm tracks, blocking and low-frequency anomalies in a primitive equation model. *J. Atmos. Sci.*, **50**, 3148-3163.

Frederiksen, J.S., and C.S. Frederiksen, 1997: Mechanism of the formation of intraseasonal oscillations and Australian monsoon disturbances: the roles of convection, barotropic and baroclinic instability. *Contrib. Atmos. Phys.*, **70**, 39-56.

Frederiksen, J.S., and G. Branstator, 2001: Seasonal and intraseasonal variability of large-scale barotropic modes. *J. Atmos. Sci*., **58**, 50-69.

IOCI 2002: *Climate variability and change in south west Western Australia.* Indian Ocean Climate Initiative Panel, Department of Environment, Water and Catchment Protection, Perth, W.A., September, 34 pp.

Kalnay E.M. et al., 1996: The NCEP/NCAR 40-year reanalysis project. *Bull Am Meteorological Soc*, **77**, 437-471.

Kanamitsu, J., 1975: On numerical prediction over a global tropical belt. Ph.D. thesis, Dept of Meteor., Florida State University, Tallahassee, FL 32304, 281 pp.

Kidson, J.W., 1988: Interannual variations in the Southern Hemisphere circulation. *J. Climate,* **1,** 1177-1198.

Knutson, T.R, and S. Manabe, 1998: Model assessment of decadal variability and trends in the tropical Pacific Ocean. *J. Climate,* **11,** 2273-2295.

Kuo, H.L., 1974: Further studies of the parameterization of the influence of cumulus convection on large scale flow. *J.Atmos.Sci.*, **31**, 1232-1240.

Krishnamurti, T.N., M. Kanamitsu, R. Godbole, C.B. Chang, F. Carr, and J. Chow, 1976: Study of a monsoon depression (II), Dynamical structure. *J. Meteor. Soc. Japan*, **54**, 208-225.

Lee, S., 1995: Linear modes and storm tracks in a 2-level primitice equation model. *J.Atmos.Sci.*, **52**, 1841-1862.

Marshall, G.J., P.A. Stott, J. Turner, W.M. Turner, J.C. King and T.A. Lachlan-Cope, 2004: Causes of exceptional atmospheric circulation changes in the Southern Hemisphere. *Geophys. Res. Lett.,* **31,** L14205, doi: 10.1029/1004GL019952.

Meehl, G.A., and W.M. Washington, 1996: El Nino-like climate change in a model with increased atmospheric CO_2 concentration. *Nature,* **382,** 56-60.

Molinari, J., 1985: A general form of Kuo's cumulus parameterization. *Mon.Wea.Rev.*, **113**, 1411-1416.

Neelin, K.K., I.M. Held, and K.H. Cook, 1987: Evaporation-wind feedback and low-frequency variability in the tropical atmosphere. *J.Atmos.Sci.*, **44**, 2341-2348.

Nicholls, N., 1989: Sea surface temperatures and Australian winter rainfall. *J. Climate*, **2,** 965-973.

Nitta, T., and S. Yamada, 1989: Recent warming of tropical sea surface temperature and its relationship to the Northern Hemisphere circulation. *J. Meteor. Soc. Japan*, **67,** 375-383.

Phillips, N.A., 1954: Energy transformations and meridional circulations associated with simple baroclinic waves in a two-level, quasi-geostrophic model. *Tellus*, **6,** 273-286.

Power, S., T. Casey, C. Folland, A. Colman and V. Mehta, 1999: Interdecadal modulation of the impact of ENSO on Australia. *Clim. Dyn.*, **15,** 319-324.

Sadler, B.S., G.W. Mauger and R.A. Stokes, 1988: The water resources implications of a drying climate in south-west Western Australia. In *Greenhouse: Planning for Climate Change*, 296-311, ed. G.I. Pearman, Commonwealth Scientific and Industrial Research Organisation, Australia, 752 pp.

Simmons, A.J., J.M. Wallace, and G.W. Branstator, 1983: Barotropic wave propagation and instability, and atmospheric teleconnection patterns. *J.Atmos.Sci.*, **40**, 1363-1392.

Smith, I.N., 1994: Indian Ocean sea-surface temperature patterns and Australian winter rainfall. *Int. J. Climatol.*, **14,** 287-305.

Smith, I.N., 2004: Trends in Australian rainfall – are they unusual? *Aust. Met. Mag.*, **53,** 163-173.

Smith, I.N., P. McIntosh, T.J. Ansell, C.J.C. Reason and K. McInnes, 2000: South-west Western Australian winter rainfall and its association with Indian Ocean climate variability. *Int. J. Climatology*, **20,** 1913-1930.

Smith, I.N. and J. Syktus, 2005: The potential impact of changes in Antarctic sea ice concentration on Southern Hemisphere climate. In preparation.

Trenberth, K. E., 1990: Recent observed interdecadal climate changes in the Northern Hemisphere. *Bull. Amer. Meteor. Soc.*, **71,** 988-993.

Whitaker, J.S. and A. Barcilon, 1992: Type B cyclogenesis in a zonally varying flow. *J. Atmos. Sci.*, **49,** 1877-1862.

Whitaker, J.S. and R.M. Dole, 1995: Organization of storm tracks in a zonally varying flow. *J. Atmos. Sci.*, **52,** 1178-1191.

Zhang, Y., J.M. Wallace and D.S. Battisti, 1997: ENSO-like variability: 1900-93. *J. Climate*, **10,** 1004-1020.

Table 1. Periods T_r^d, growth rates ω_i^d and e-folding times τ_i^d of the 20 fastest growing modes for the 1949-68 basic state, their mode number and class of mode. Also shown are the largest pattern correlations A_c between a given mode and the modes for 1975-94 basic state and, in brackets, the 1975-94 mode for which the pattern correlation is largest. The modes are classified as Southern Hemisphere monopole cyclogenesis (shC), Northern Hemisphere monopole cyclogenesis (nhC), Southern Hemisphere dipole cyclogenesis (shDC), Southern Hemisphere blocking (shB), Antarctic teleconnection pattern (aTP), Northern Hemisphere tropical wave (nhTW) and Southern Hemisphere north-west cloud band (shNWCB).

Class	**Mode 1949-68**	T_r^d **(days)**	ω_i^d **(day^{-1})**	τ_i^d **(days)**	A_c	**Mode 1975-94**
shC	1	1.20	0.4250	2.353	0.9148	9
nhC	2	2.77	0.4006	2.500	0.9340	1
shC	3	0.98	0.3930	2.544	0.9564	20
shC	4	2.29	0.3768	2.654	0.7566	15
shC	5	2.64	0.3678	2.719	0.7655	13
aTP	6	13.08	0.3624	2.759	0.9416	3
nhC	7	3.57	0.3497	2.860	0.9474	2
shC	8	7.40	0.3495	2.861	0.8342	4
shDC	9	2.99	0.3328	3.005	0.5733	31
shC	10	3.10	0.3308	3.023	0.7255	19
shDC	11	5.22	0.3184	3.141	0.8468	6
shC	12	2.01	0.3182	3.142	0.5676	25
shDC	13	3.50	0.3176	3.149	0.5631	19
nhC	14	3.20	0.3100	3.226	0.8613	5
shDC	15	2.57	0.3095	3.231	0.5385	16
shC&nhC	16	3.75	0.3007	3.326	0.5531	27
shDC	17	2.36	0.2948	3.392	0.3998	25
shC	18	1.99	0.2942	3.398	0.6345	61
shC	19	1.77	0.2926	3.417	0.6324	61
shDC&nhC	20	4.13	0.2925	3.419	0.5659	8

Table 2. As in Table 1 but for modes growing on the 1975-94 basic state (and with the roles of the two basic states interchanged).

Class	**Mode 1975-94**	T_r^d **(days)**	ω_i^d **(day^{-1})**	τ_i^d **(days)**	A_c	**Mode 1949-68**
nhC	1	2.64	0.4160	2.404	0.9340	2
nhC	2	3.50	0.3696	2.706	0.9474	7
aTP	3	17.48	0.3606	2.773	0.9416	6
shB	4	8.02	0.3317	3.015	0.8342	8
nhC	5	3.13	0.3212	3.113	0.8613	14
shDC	6	5.08	0.3101	3.225	0.8468	11
nhTW	7	3.83	0.3071	3.256	0.7959	22
shDC&nhC	8	3.86	0.2829	3.535	0.5659	20
shC	9	1.30	0.2824	3.541	0.9148	1
nhC	10	4.10	0.2768	3.613	0.8316	33
aTP	11	21.26	0.2700	3.703	0.8524	26
shNWCB	12	8.19	0.2624	3.812	0.8036	43
shC	13	2.83	0.2583	3.871	0.7655	5
nhC	14	4.95	0.2578	3.879	0.5734	46
shC	15	2.51	0.2535	3.944	0.7566	4
shDC	16	2.39	0.2440	4.098	0.5385	15
shC&nhC	17	5.96	0.2391	4.180	0.8629	42
shDC	18	2.06	0.2392	4.181	0.5319	28
shC	19	3.31	0.2342	4.270	0.7255	10
shC	20	1.03	0.2288	4.370	0.9564	3

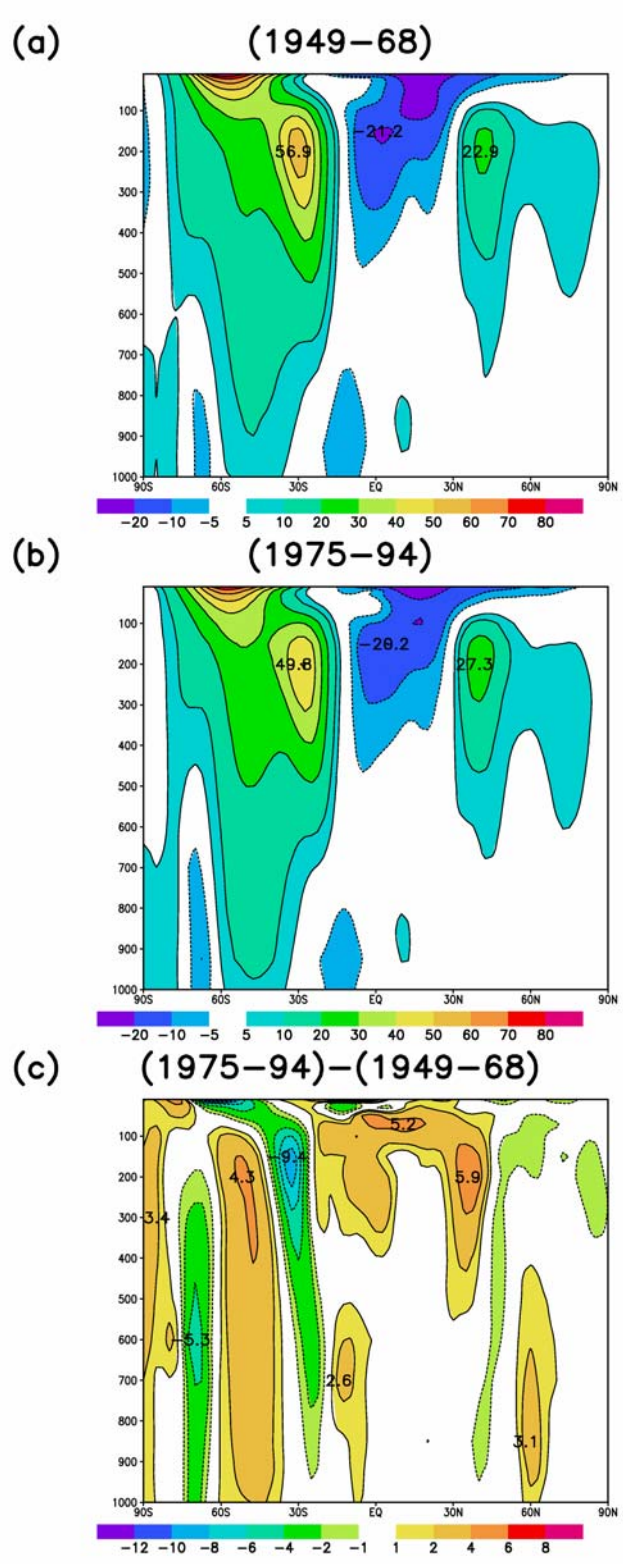

Figure 1. Vertical cross-section of July zonal wind (ms^{-1}) averaged between 100° and 130° E as a function of latitude and pressure (in hPa) for the 1949-68 basic state (a), the 1975-94 basic state (b) and their difference (1975-94)-(1949-68) (c). Contour intervals are 10, 10 and 2 ms^{-1} respectively, but here, and in subsequent Figures, may be closer spaced near 0 as shown on bars.

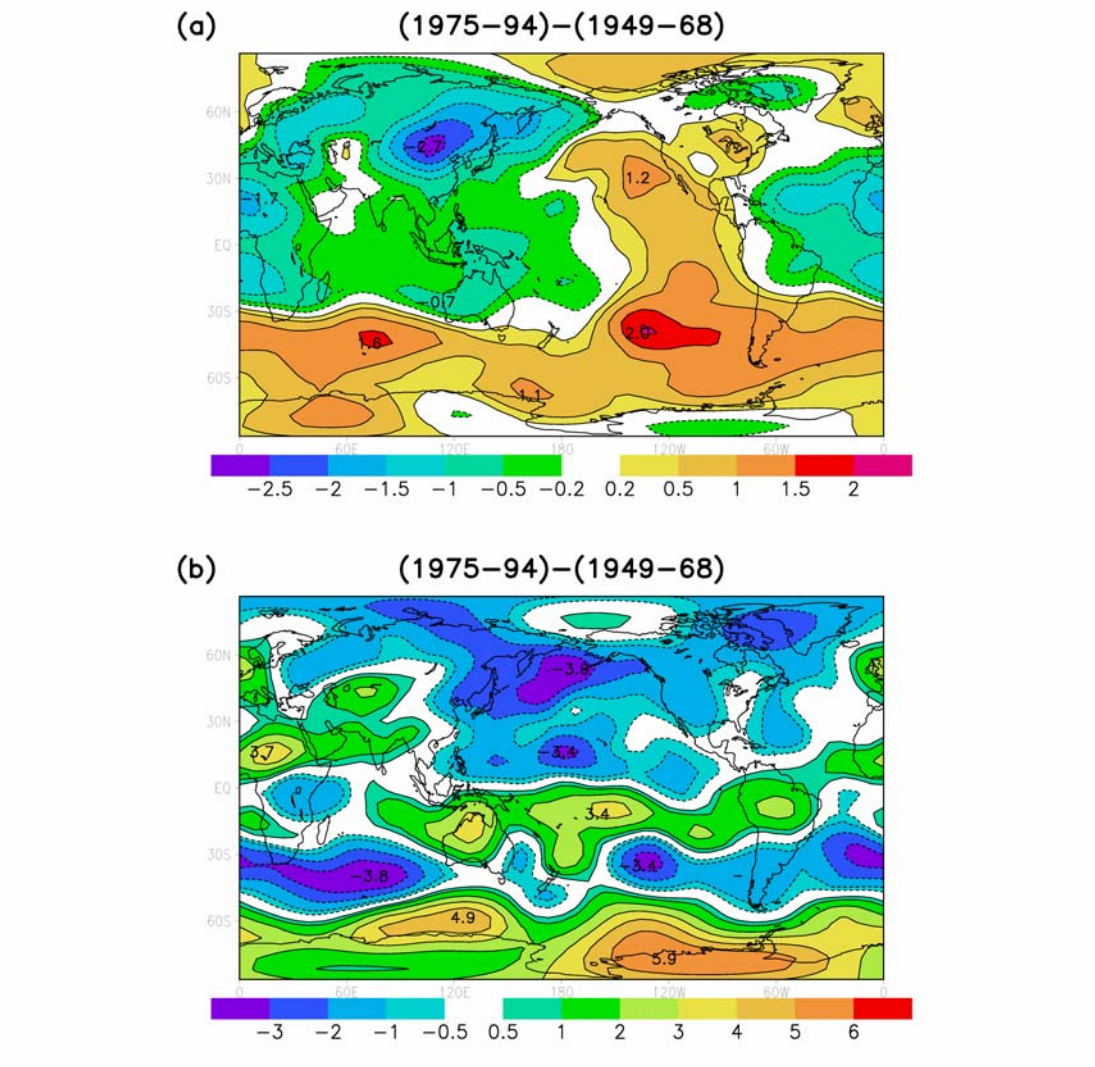

Figure 2. Horizontal latitude-longitude plot of the July (1975-94)-(1949-68) difference in the vertically averaged potential temperature (*K*) (a) and the corresponding vertically averaged streamfunction difference ($km^2\ s^{-1}$). Contour intervals are 0.5 K and 1 $km^2\ s^{-1}$ respectively.

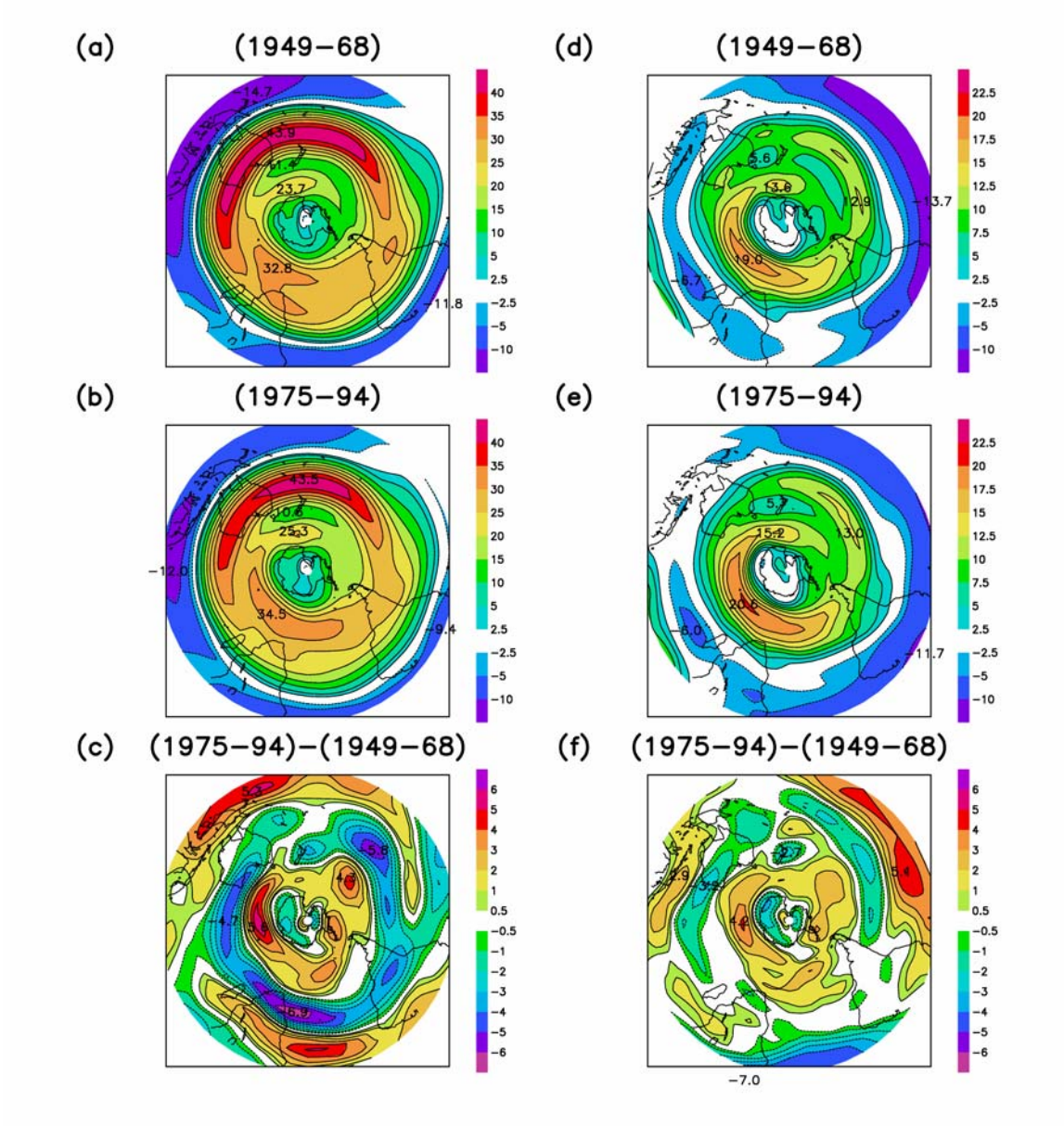

Figure 3. The SH upper-level basic state zonal wind $u^{(1)d}\,(\mathrm{m\,s^{-1}})$, taken from 300 hPa observations, for July 1949-68 (a), 1975-94 (b) and the (1975-94)-(1949-68) difference (c). The lower-level basic state zonal wind $u^{(3)d}\,(\mathrm{m\,s^{-1}})$, taken from 700 hPa observations, for July 1949-68 (d), 1975-94 (e) and the (1975-94)-(1949-68) difference (f). Contour intervals are 5, 5, 1, 2.5, 2.5 and 1 $\mathrm{ms^{-1}}$ respectively.

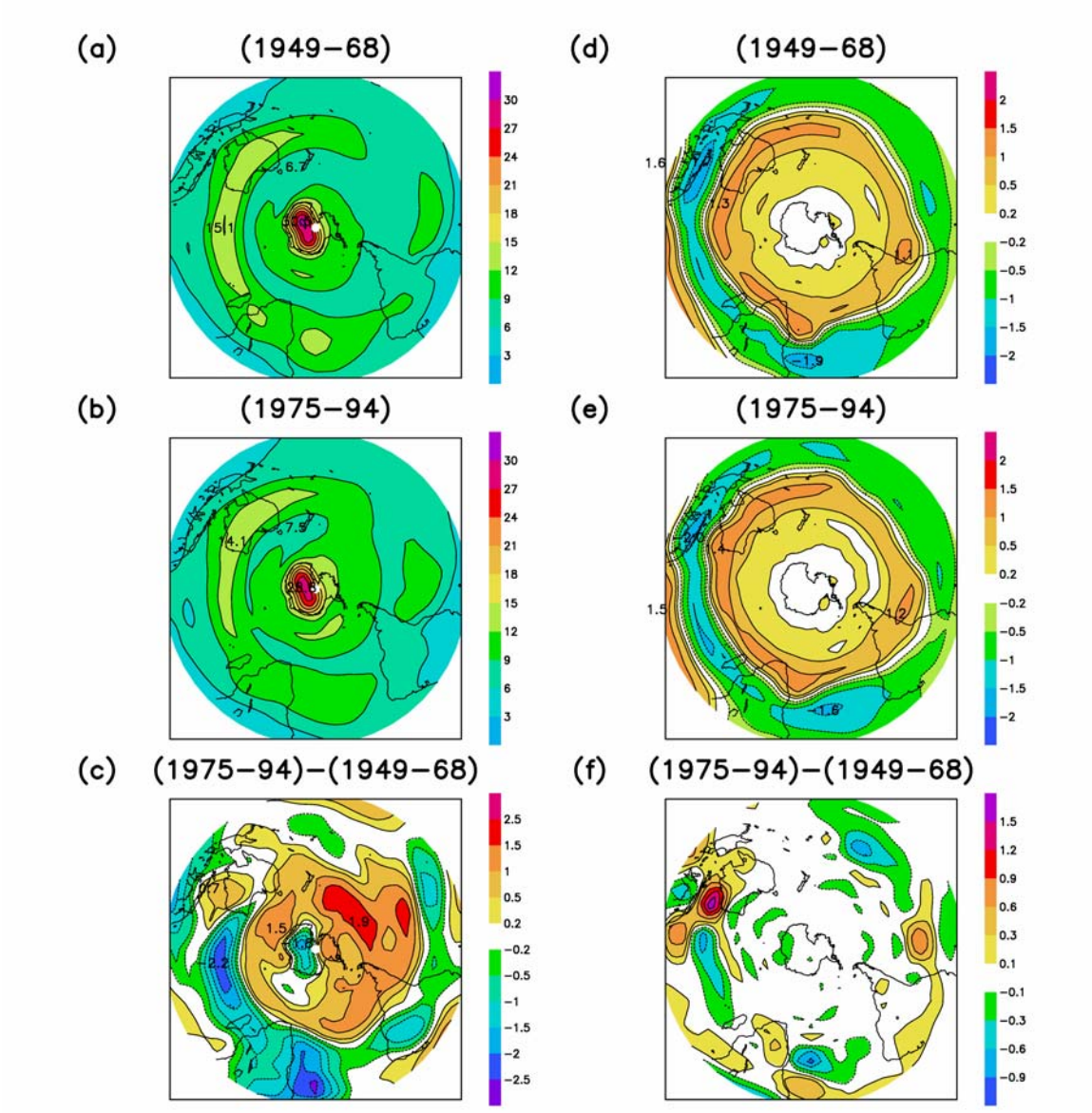

Figure 4. The SH moist static stability parameter $\sigma_m^d = \sigma^d - s^d$ (K) of Eq.(3.2) for July 1949-68 (a), 1975-94 (b) and the (1975-94)-(1949-68) difference (c). The SH evaporation-wind structure function f_u^d (g kg^{-1}) of Eq.(2.3a) for July 1949-68 (d), 1975-94 (e) and the (1975-94)-(1949-68) difference (f). Contour intervals are 3, 3, 0.5, 0.5, 0.5 and 0.3 respectively.

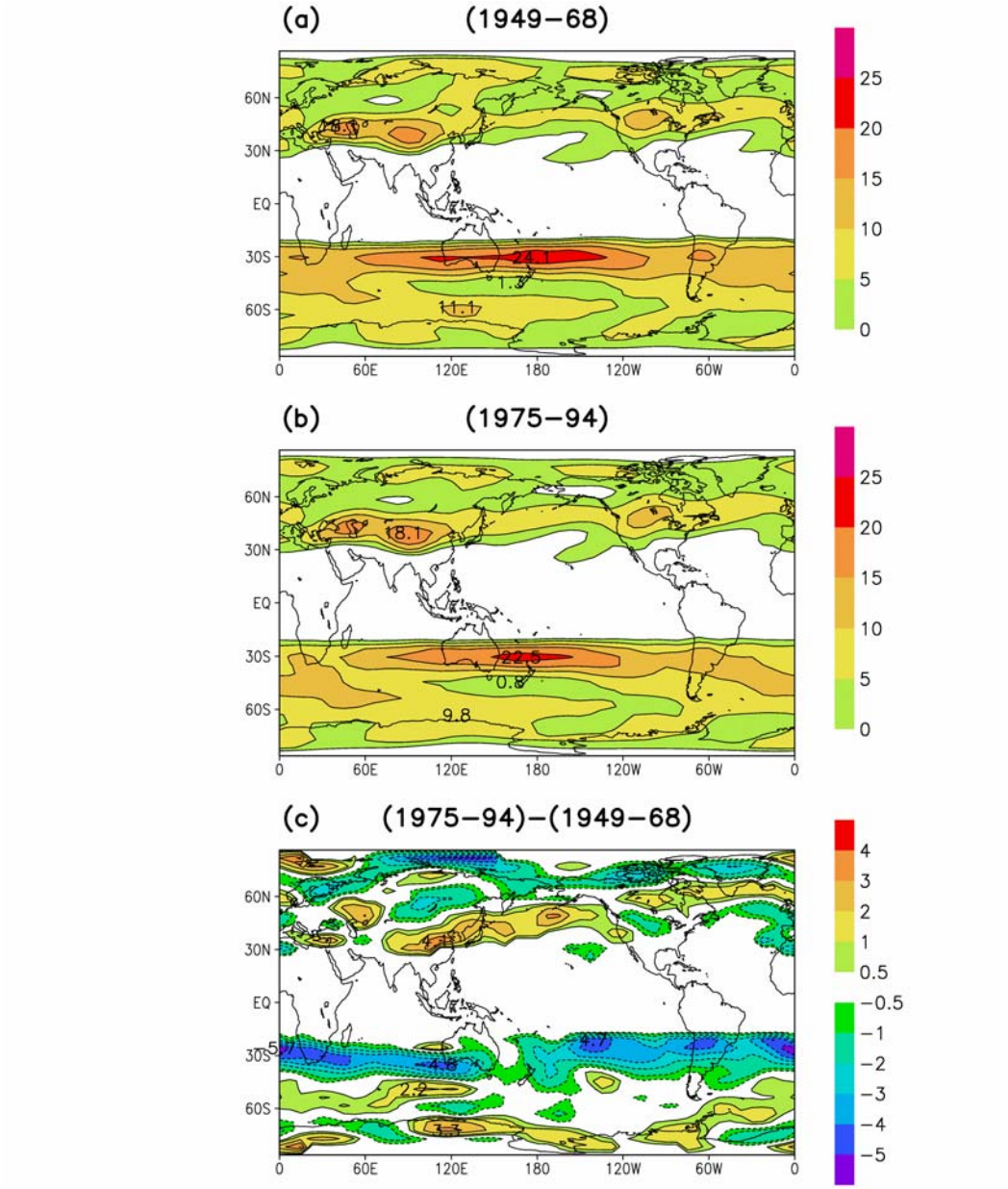

Figure 5. The global generalized Phillips instability criterion of Eq.(4.1), with the moist static stability $\overline{\sigma}_m^d$, in units of ms^{-1} for July 1949-68 (a), 1975-94 (b) and the (1975-94)-(1949-68) difference (c). Contour intervals are 5, 5 and 1 respectively.

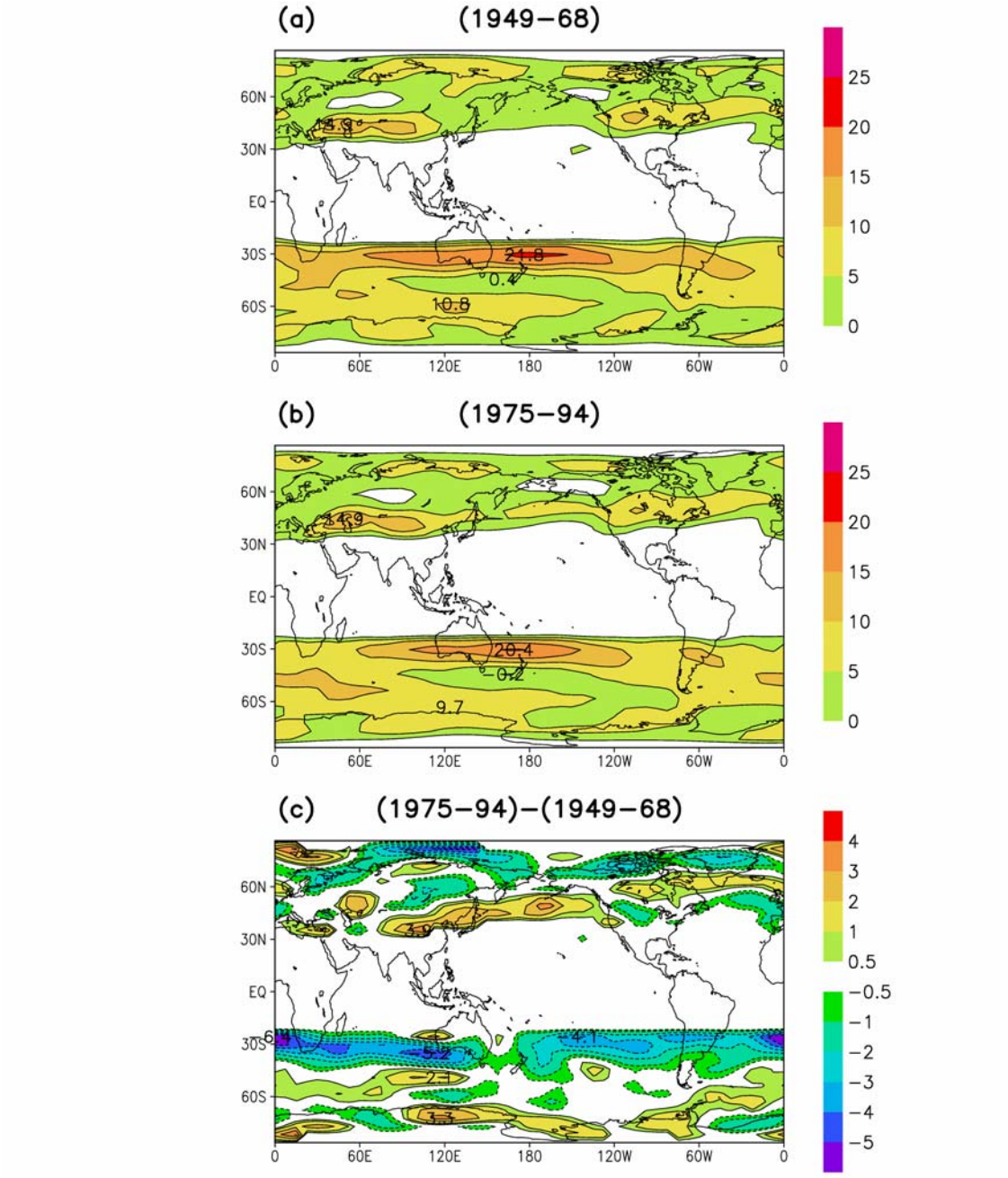

Figure 6. As in Fig.5 with the dry static stability $\overline{\sigma}^{d}$.

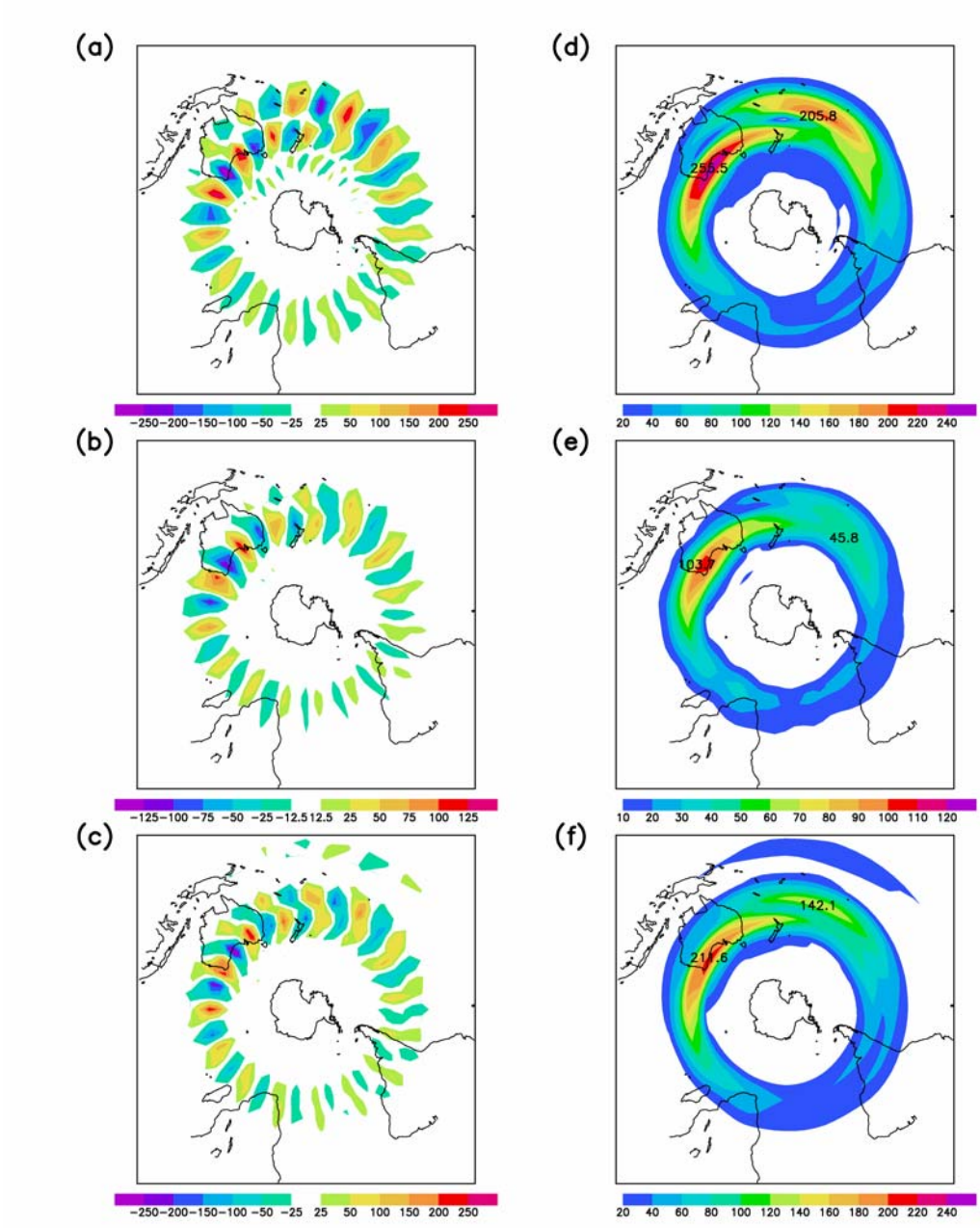

Figure 7. Shown in arbitrary units are (a) the upper-level streamfunction $\left(\psi^1\right)$, (b) the lower-level streamfunction $\left(\psi^3\right)$and (c) the upper-level divergence $(-D)$ for the fastest growing SH cyclogenesis mode, mode 1, for the July 1949-68 basic state and the corresponding RPEA of (d) the upper-level streamfunction $\left(\psi^1\right)$, (e) the lower-level streamfunction $\left(\psi^3\right)$and (f) the upper-level divergence $(-D)$. Contour intervals are 50, 25, 50, 20, 10, and 20 respectively and the divergence has been scaled by 10^{-2}.

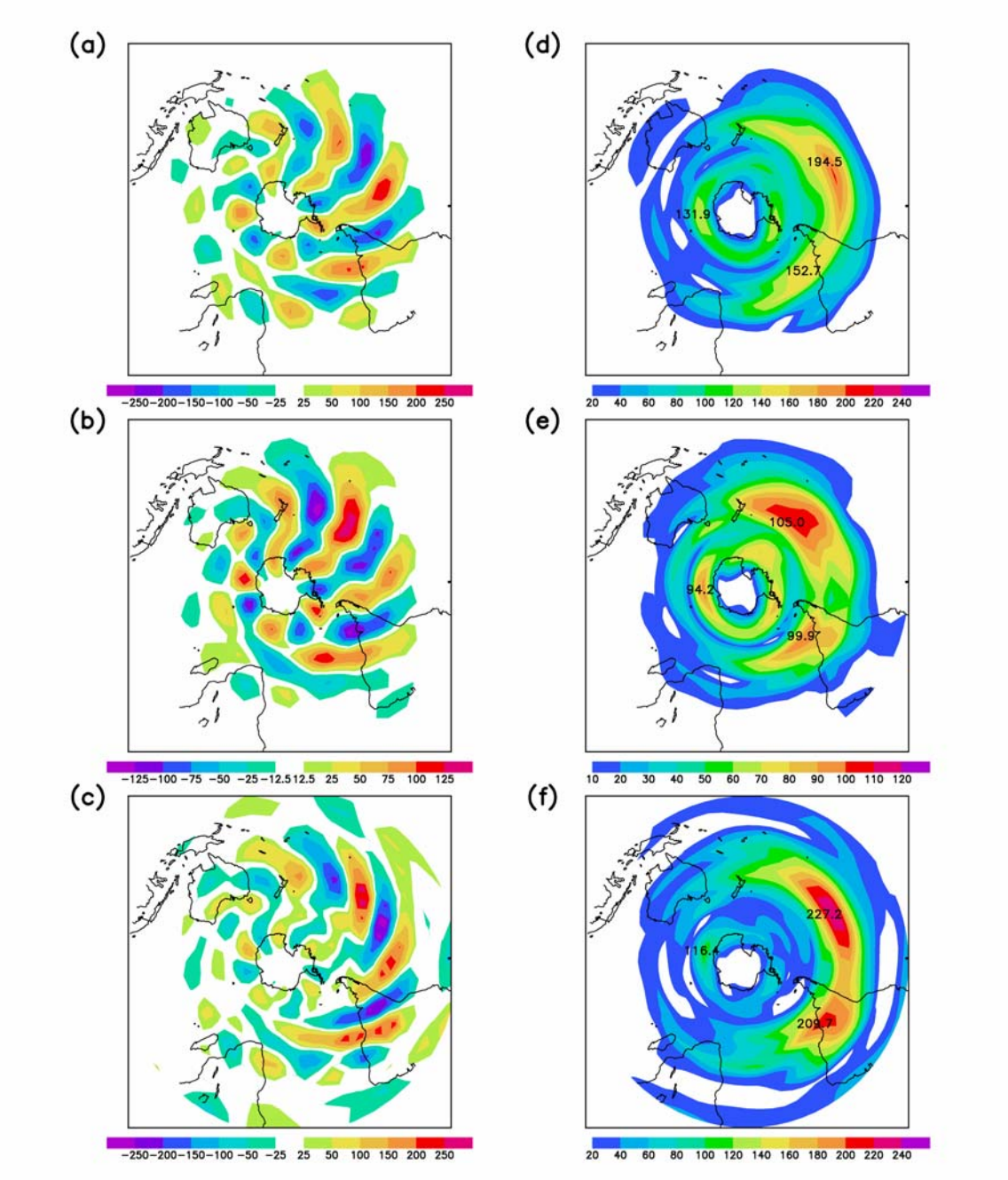

Figure 8. As in Fig.7 but for the fastest growing SH cyclogenesis mode, mode 8, for the July 1975-94 basic state and the divergence scaled by $5x10^{-2}$.

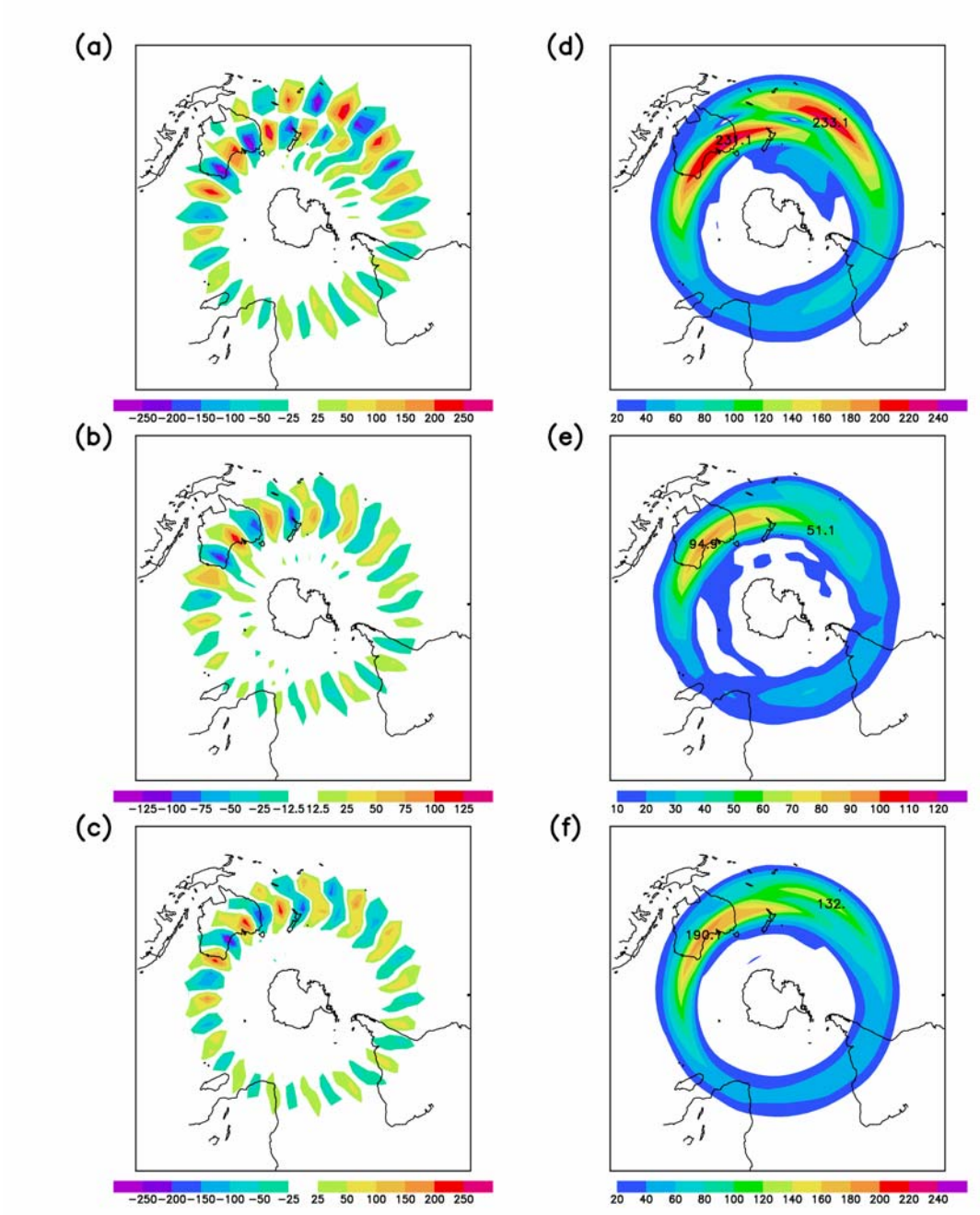

Figure 9. As in Fig.7 but for the second fastest growing SH cyclogenesis mode, mode 9, for the July 1975-94 basic state.